JACS
JOURNAL OF THE AMERICAN CHEMICAL SOCIETY
Article
pubs.acs.org/JACS

A Computational Mechanistic Study of an Unprecedented Heck-Type Relay Reaction: Insight into the Origins of Regio- and Enantioselectivities

Yanfeng Dang,[†] Shuanglin Qu,[†] Zhi-Xiang Wang,*[,†,§] and Xiaotai Wang*[,‡]

[†]School of Chemistry and Chemical Engineering, University of the Chinese Academy of Sciences, Beijing 100049, People's Republic of China

[‡]Department of Chemistry, University of Colorado, Denver, Campus Box 194, P.O. Box 173364, Denver, Colorado 80217-3364, United States

[§]Collaborative Innovation Center of Chemical Science and Engineering, Tianjin 300072, People's Republic of China

Supporting Information

ABSTRACT: Density functional theory (DFT) calculations (B3LYP and M06) have been utilized to study a newly reported Heck-type reaction that uses an allylic or alkenyl alcohol as substrate and palladium as catalyst in the form of a chelate with a chiral pyridine oxazoline (PyrOx) ligand. The reaction not only controls the regio- and enantioselectivities of arylation of the C=C bond, but also forms the carbonyl functionality up to four bonds away from the aryl substituent via tandem C=C bond migration and enol-to-keto conversion. Computations performed on representative reaction systems allow us to propose a detailed mechanism with several key steps. Initial oxidation of palladium(0) by aryldiazonium generates active arylpalladium(II) species that bind the C=C bond of an allylic or alkenyl alcohol. The activated C=C bond inserts into the palladium−aryl moiety to attain aryl substitution and a chiral carbon center, and the resulting complex undergoes β-hydride elimination to give a new C=C bond that can repeat the insertion/elimination process to move down the carbon chain to form an enol that tautomerizes to a highly stable carbonyl final product. The calculations reveal that the C=C bond migratory insertion step determines both the regioselectivity and the enantioselectivity of arylation, with the former arising mainly from the electronic effect of the hydroxyl group on the charge distribution over the C=C bond and the latter originating from a combination of steric repulsion, trans influence, and C−H/π dispersion interactions.

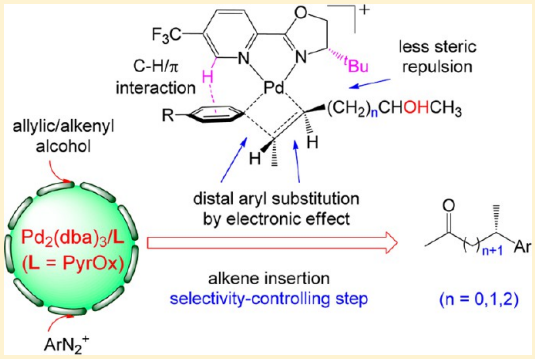

1. INTRODUCTION

The palladium-catalyzed Heck coupling reaction creates new carbon−carbon bonds and has wide use in chemical synthesis, especially of complex natural products (Scheme 1).[1−5] Mechanistically, an initial oxidative addition of a vinyl or aryl halide to an unsaturated Pd(0) complex results in a Pd(II) species, which then forms a π complex with the alkene substrate. The alkene undergoes migratory insertion into the palladium−carbon bond, followed by β-hydride elimination, to give the substituted alkene product. The catalyst is regenerated via a base-aided reductive elimination of HX.[5−14]

Because both the alkene insertion and the β-hydride elimination steps are site-selective, in practicing classical Heck reactions, electronically biased alkenes, such as methyl vinyl ketone where the C=C bond is polarized through conjugation with the C=O bond, are generally employed to control regioselectivity.[3,5] The obligatory use of such alkenes, however, limits the range of transformations available. A recent important development in using less electronically biased alkenes for Heck-type reactions was reported by Sigman et al.,[15] which employs a chiral pyridine oxazoline (PyrOx) ligand[16] to support the palladium catalyst, and aryldiazonium salts as the arene source. This methodology allows an allylic or alkenyl alcohol[17] substrate to undergo a Heck-type relay reaction, as summarized in Scheme 2.[15] The reaction is not only regioselective with aryl substitution on the C=C bond site that is more remote (or distal) from the alcohol end, but it is also enantioselective to the prochiral C=C bond. Furthermore, it can form a carbonyl functionality up to four bonds away from the aryl substituent apparently through C=C bond migration and enol-to-keto conversion. This work represents a breakthrough in synthetic methodology, as it generates a carbon−carbon bond with a chiral center both regioselectively and enantioselectively, as well as a functionality remote from the chiral center; few reactions could achieve such three results all together.[18] It also gives other intriguing results such as that the racemic nature of an alkene substrate does not bias enantioselection, that (*Z*)- and

Received: October 2, 2013
Published: December 31, 2013

© 2013 American Chemical Society

dx.doi.org/10.1021/ja410118m | J. Am. Chem. Soc. 2014, 136, 986−998

Scheme 1. The Heck Reaction (A) and Its Mechanism (B)

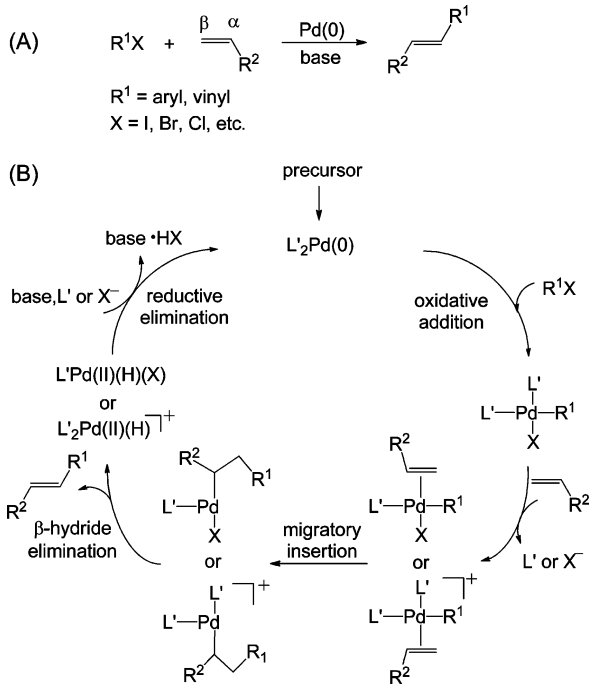

Scheme 2. Regio- and Enantioselective Heck Arylations of Allylic and Alkenyl Alcohols

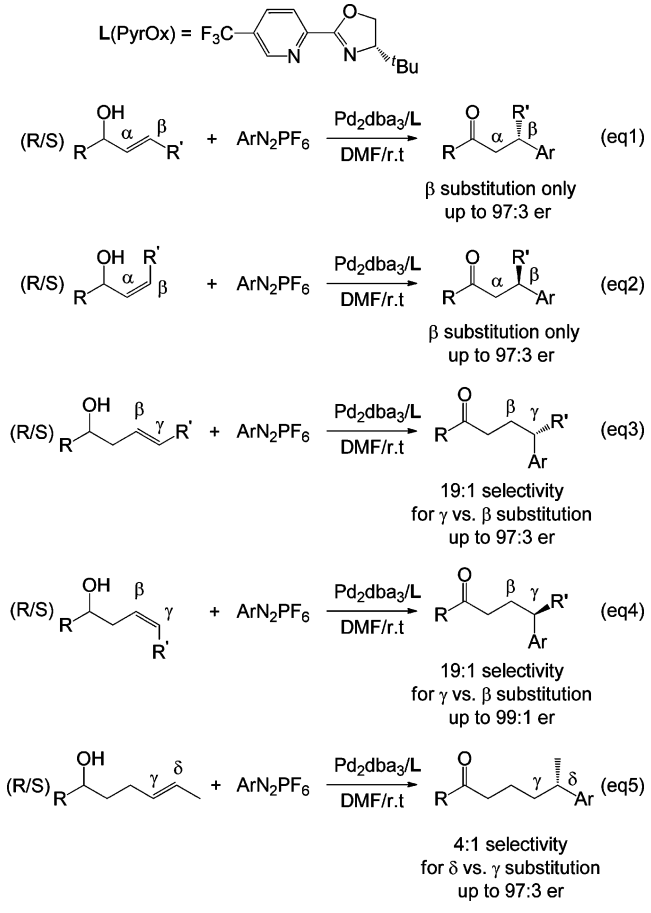

(*E*)-alkenes give opposite enantiomers of product, and that the distal regioselectivity of arylation decreases with increasing

Scheme 3. Metal Migration through the Carbon Chain

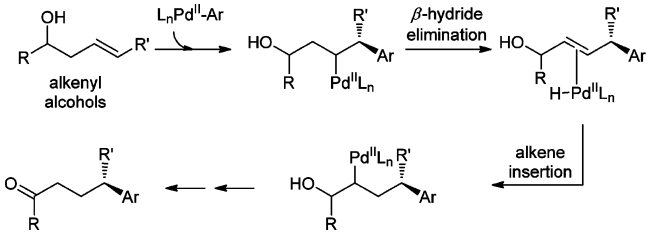

carbon chain length of the alkenyl alcohol. Although migration of the metal fragment through the carbon chain was proposed to account for the C=C bond relay (Scheme 3),[15,19−21] the detailed mechanism of this remarkable catalytic reaction, particularly origins of the regio- and enantioselectivities, has not been explored at the outset of this work.

We have performed density functional theory (DFT) calculations on this unprecedented Heck-type relay reaction, using representative reaction systems. The computational work presented here constitutes a plausible mechanism, explains the C=C bond relay, and elucidates the origins of the observed regio- and enantioselectivities.

2. COMPUTATIONAL METHODS

Geometry optimizations and frequency calculations were performed at the B3LYP/BS1[22] level in DMF solution using the SMD[23] solvation model with default convergence criteria, BS1 designating a mixed basis set of SDD[24] for palladium, and 6-31G(d,p) for other atoms. Frequency outcomes were examined to confirm stationary points as minima (zero imaginary frequencies) or transition states (one imaginary frequency). Because the M06[25] functional includes noncovalent interactions and can give accurate energies for organotransition metal systems,[26,27] we carried out single-point energy calculations for all of the B3LYP/BS1-optimized structures at the M06/BS2 level with solvation effects modeled by SMD in DMF, BS2 denoting a mixed basis set of SDD for palladium, and 6-311++G(d,p) for other atoms. Numerous studies have demonstrated the validity of this B3LYP/M06 combined method for organotransition metal systems, as it gives computational results that correlate well with experimental obervations.[28−30] The B3LYP/BS1-calculated frequencies were used to obtain zero-point energy-corrected enthalpies and free energies at 298.15 K and 1 atm in DMF solution. Natural bond orbital (NBO) analyses were performed at the M06/BS2 level in DMF solution with the SMD model on selected systems. Free energies (kcal/mol) obtained from the M06/BS2//B3LYP/BS1 calculations were discussed, and enthalpies (kcal/mol) were given for reference. For comparison purposes, the key transition states obtained with M06/BS2//B3LYP/BS1 calculations were also subjected to calculations with M06/BS2//M06/BS1. All calculations were performed with Gaussian 09.[31]

3. RESULTS AND DISCUSSION

The mechanism proposed on the basis of our DFT calculations includes the following key steps: (1) oxidation of palladium(0) by aryldiazonium to generate an arylpalladium(II) complex as

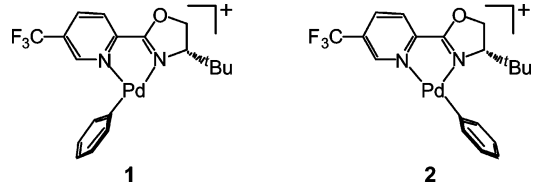

Figure 1. Phenylpalladium(II) complexes **1** and **2**.

dx.doi.org/10.1021/ja410118m | J. Am. Chem. Soc. 2014, 136, 986−998

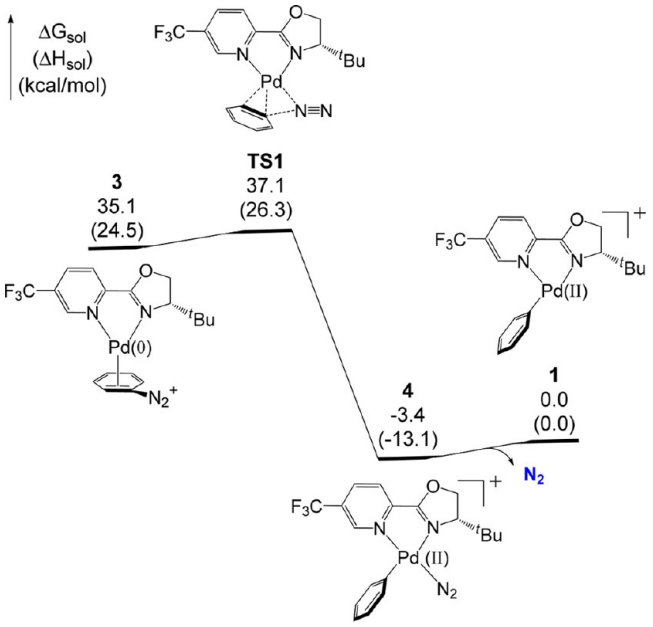

Figure 2. Free energy profile for the oxidation of Pd(0) to Pd(II) by phenyldiazonium. Energies are relative to complex **1** and are mass-balanced (similarly hereinafter).

the active species, (2) attack on the palladium(II) center by the C=C bond of an allylic or alkenyl alcohol to afford a π complex, (3) migratory insertion of the C=C bond into the palladium−aryl moiety to attain aryl substitution and a chiral carbon center, and (4) β-hydride elimination to give a new C=C bond that can repeat the insertion/elimination process to move toward the alcohol end to finally form a carbonyl product via enol-to-keto conversion. The regio- and enantioselectivities arise in steps 3 and 4. The details of these and other processes will be discussed in the following sections.

3.1. Oxidative Initiation. Equation eq6 represents a plausible reaction for the initiation of the precatalyst, in which the Pd(0) complex $Pd_2(dba)_3$ undergoes ligand substitution for PyrOx, followed by oxidation by the diazonium cation $[PhN_2]^+$ of $[PhN_2][PF_6]$ to form Pd(II) complexes **1** and **2**, the active catalytic species (Figure 1). Note that **1** and **2** are cationic complexes balanced by the counterion PF_6^- that is assumed to be a spectator ion and hence not considered in the calculations.[32]

$$\frac{1}{2}Pd_2dba_3 + PyrOx + [PhN_2]^+ \rightarrow [(PyrOx)PdPh]^+(\mathbf{1}/\mathbf{2}) + \frac{3}{2}dba + N_2 \quad \text{(eq6)}$$

The formation of diastereomeric **1** and **2** arises from the asymmetric nature of the ligand PyrOx. The reaction has a large thermodynamic driving force, with $\Delta G^\circ = -25.0$ kcal/mol approximately for both **1** and **2**, and the transition states (TSs) and intermediates for the most favorable pathways to **1** and **2** have closely similar energies (Supporting Information, Figures S1 and S2). Thus, we cannot rule out either of them at this stage and should consider both of them for subsequent reactions. The free energy profile for the oxidation step leading to **1** is shown in Figure 2 as an example, which indicates that the oxidation of the palladium(0) phenyldiazonium π complex **3** to the palladium(II) phenyl dinitrogen complex **4** is not only exergonic ($\Delta G^\circ = -38.5$ kcal/mol), but also facile with a low activation energy (2.0 kcal/mol). Dissociation of N_2 from **4** affords the 14-electron phenylpalladium(II) complex **1** with a T-shaped coordination geometry. Complex **1** should occur irreversibly in significant quantities because of the large thermodynamic driving force and the evolution of N_2 as a gas.

3.2. Reactions with Allylic Alcohols. *Mechanism.* We have chosen to model, without truncation, the actually performed reactions with a view to elucidating the mechanism and origins of regio- and enantioselectivities (Scheme 4).[15] The experimental runs used racemic (*E*)-(*R*/*S*)-**sub1**, so we considered (*E*)-(*S*)-**sub1** first for DFT computations. Given that (*E*)-(*S*)-**sub1** is an unsymmetrical alkene, we have optimized four of its possible π complexes with each of **1** and **2**, two of them continuing on β-insertion (Scheme 5) and the other two continuing on α-insertion (Supporting Information, Scheme S1).

Experimentally, only the β-substituted ketones **1a** and **1b** deriving from the β-insertion mechanism were observed as the final products (Scheme 4). Scheme 5 summarizes four possible alkene β-insertion pathways, each of which would lead to the final product **1a**/**1b**/**1c**. For each of these pathways, the alkene migratory insertion transition state (**TS2**/**TS3**/**TS4**/**TS5**) determines both the regio- and the enantioselectivities (see below), and the resulting palladium alkyl complex (**6**/**8**/**10**/**12**) contains a Pd−η^2-phenyl bond, fulfilling a 16-electron valence shell on the Pd(II) center. Analogous palladium complexes with the Pd−η^2-phenyl coordination mode have been computed previously.[6,7] Path 1A, the most favorable route, bifurcates at complex **6** via site-selective β-elimination onto paths 1A1 and 1A2, which lead respectively to the (*S*)-β-phenyl ketone **1a** and typical Heck product **1c**.

The free energy profiles of paths 1A1 and 1A2 from **6** onward are shown in Figure 3. Complex **6** contains two different β−hydrogen atoms marked as H_a and H_b. A direct β-H_a elimination (path 1A1) would not happen to **6** because of the large Pd−C_α−C_β(a)−H_a dihedral angle (60.5°) and Pd−H_a separation (3.16 Å). Thus, we located the transition state (**TS6**) of rotation about the Pd−C_α bond, as well as the

Scheme 4. The Heck Arylation of (*E*)-Allylic Alcohol

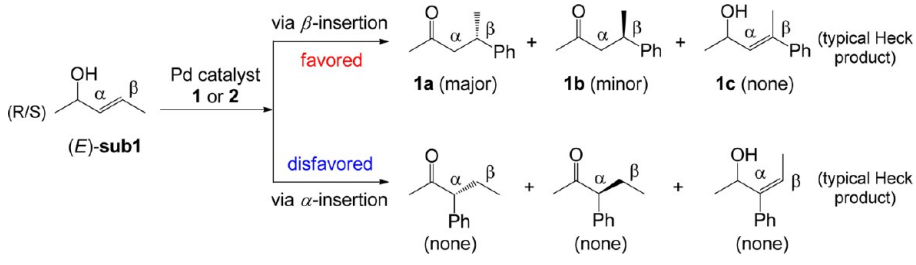

dx.doi.org/10.1021/ja410118m | J. Am. Chem. Soc. 2014, 136, 986−998

Scheme 5. Reactions of (*E*)-(*S*)-sub1 with Pd Catalyst 1 or 2 Leading to *β*-Substituted Products

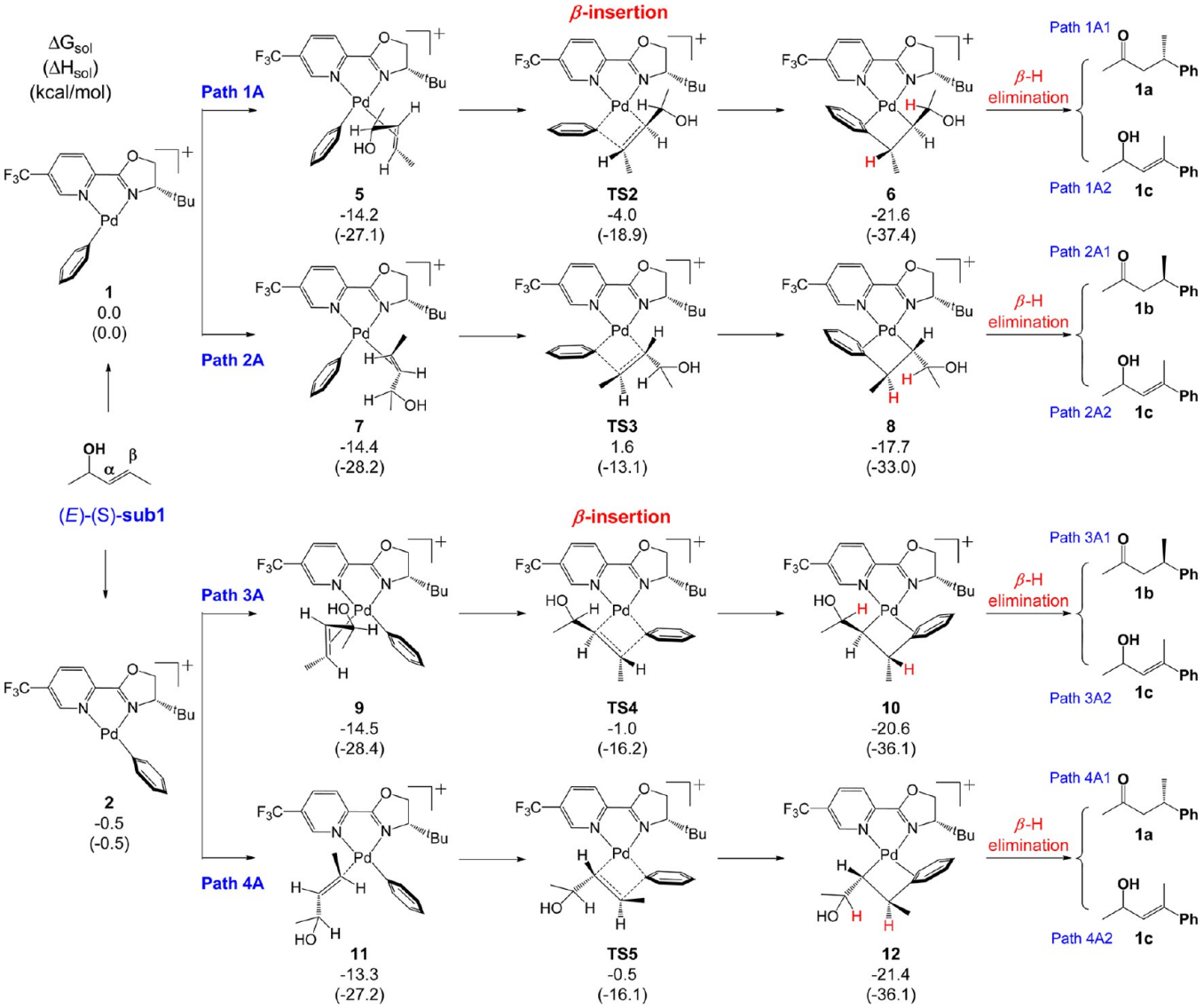

resulting isomer **13**. Complex **13** has a Pd−C_α−C_β(a)−H_a dihedral angle at 10.9° and an agostic Pd−H_a interaction at 1.73 Å, both of which would facilitate the subsequent *β*-H_a elimination via **TS7** that proceeds to complex **14** with the *π*-bound product (*S*)-enol **1d**. **TS7** is higher than **13** in electronic energy in DMF solution, but the corrected free energy of **TS7** becomes somewhat lower, which could mean a facile *β*-hydrogen elimination without much of a kinetic barrier. Complex **14** then undergoes a hydrogen elimination (or deprotonation) aided by the solvent DMF, for which we have located both the transition state **TS8** and the resulting product, a formal Pd(0) complex (**15**) with the protonated DMF (or DMF·H^+) weakly associated with the metal center mostly through electrostatic interactions. The dissociation of DMF·H^+ from **15** generates complex **16**, which undergoes substitution associatively for phenyldiazonium through the four-coordinate, tetrahedral intermediate **17** to lead to the original Pd(0) complex **3** with the release of the (*S*)-enol product **1d**. We have also considered the dissociative mechanism of enol discharge and found it less favorable.[33] The subsequent enol−keto conversion (**1d** → **1a**) is thermodynamically favorable with a large driving force (14.3 kcal/mol) due to the stability of the ketone isomer. Meantime, complex **3** proceeds via the oxidation of the Pd(0) center by the ligated diazonium cation PhN_2^+ to regenerate the active catalyst **1**, as has been characterized and discussed above (Figure 2). We now evaluate the energetics of several key steps in path 1A1. Clearly, the alkene migratory insertion (**5** → **6**) not only has the comparatively highest barrier of **TS2** (−4.0 kcal/mol), but is also irreversible (ΔG^0 = −7.4 kcal/mol), thereby determining the regio- and enantioselectivities (Scheme 5). The *β*-hydride elimination step appears to be turnover-limiting, because it has a larger free energy of activation (**6** → **TS6**, 11.2 kcal/mol) than that of the alkene insertion (**5** → **TS2**, 10.2 kcal/mol) or the deprotonation (**14** → **TS8**, 10.7 kcal/mol).

Path 1A2 leading to the typical Heck product **1c** is similar to path 1A1 (Figure 3), proceeding with rotation/isomerization of **6** to **18** via **TS9**. The conformation of **18** with the agostic Pd−H_b interaction at 1.76 Å and the Pd−C_α−C_β(b)−H_b dihedral angle at 6.2° would facilitate the subsequent *β*-H_b elimination via **TS10** to form **19**, followed by the DMF-aided deprotonation and the phenyldiazonium substitution for the *π*-bound Heck product **1c**. The high stationary points **TS9**, **TS11**, and **22** in path 1A2 are comparable in energy, and any of

dx.doi.org/10.1021/ja410118m | J. Am. Chem. Soc. 2014, 136, 986−998

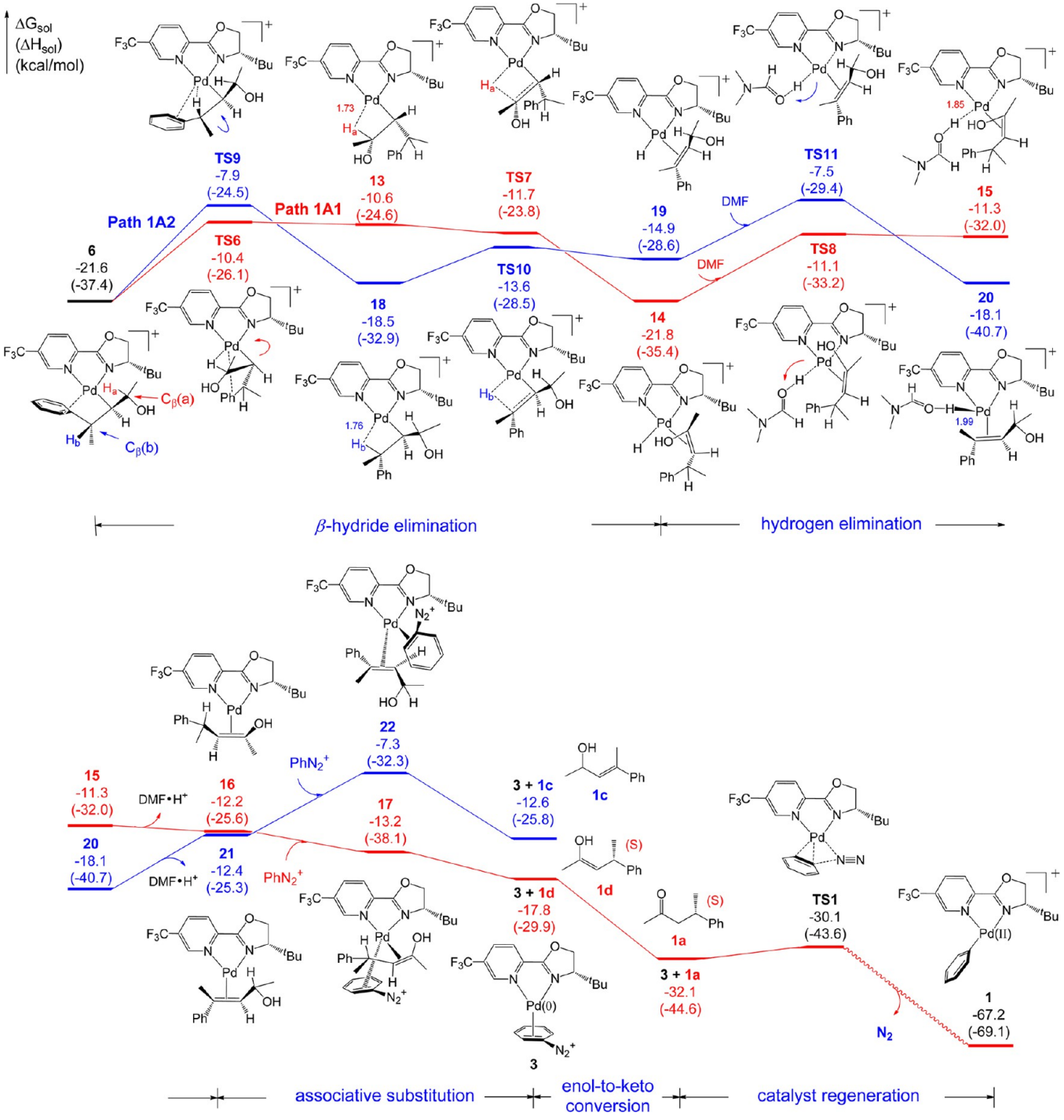

Figure 3. Free energy profiles for the reactions with (*E*)-(*S*)-**sub1** leading to the *β*-phenyl ketone **1a** (red) and the typical Heck product **1c** (blue).

them is higher than the limiting barrier **TS6** in path 1A1 by a minimum of 2.5 kcal/mol. More importantly, path 1A1 is thermodynamically more favorable than path 1A2 by 19.5 kcal/mol. Thus, there is an overwhelming preference for **1a** over **1c**, which explains why the typical Heck product **1c** was not observed experimentally.

The most favorable pathway leading to the (*R*)-*β*-phenyl ketone **1b** is path 3A1 with the alkene insertion transition state **TS4** (Scheme 5) derived from **2** (the other active catalyst). **TS4** is higher than **TS2** of path 1A1 by 3.0 kcal/mol, and the difference in energy gives a calculated enantioselectivity (>99%) in favor of **1a**, the product of path 1A1. This agrees qualitatively with the experimental enantioselectivity (**1a**:**1b** = 93:7).[15] We will next discuss the origins of the enantio- and regioselectivities by examining the structures of the key transition states and intermediates.

Origins of Regio- and Enantioselectivities. We herein examine the structures of diastereomeric **TS2** and **TS4** (Figure 4) to understand their difference in energy, from which the enantioselectivity originates favoring the (*S*)-*β*-phenyl ketone **1a** over the (*R*)-*β*-phenyl ketone **1b**. In **TS2**, the phenyl group is cis to the pyridine moiety of the ligand PyrOx, whereas in **TS4**, it is cis to the oxazoline moiety with a bulky *t*-butyl substituent. The phenyl orientation toward PyrOx is crucial

dx.doi.org/10.1021/ja410118m | J. Am. Chem. Soc. 2014, 136, 986−998

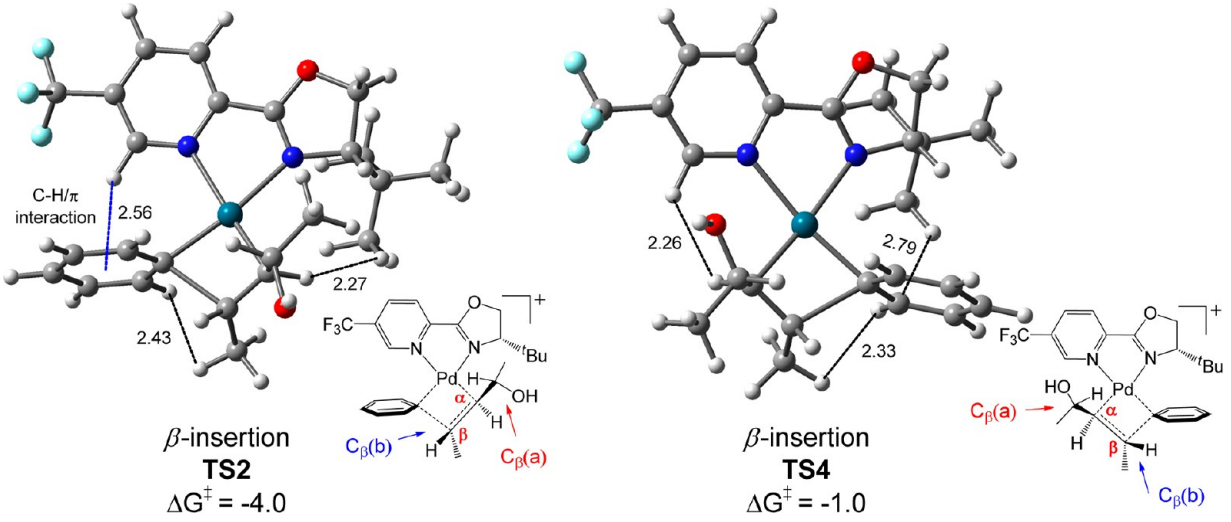

Figure 4. Optimized structures of **TS2** (leading to **1a**) and **TS4** (leading to **1b**) with selected bond distances given in angstroms.

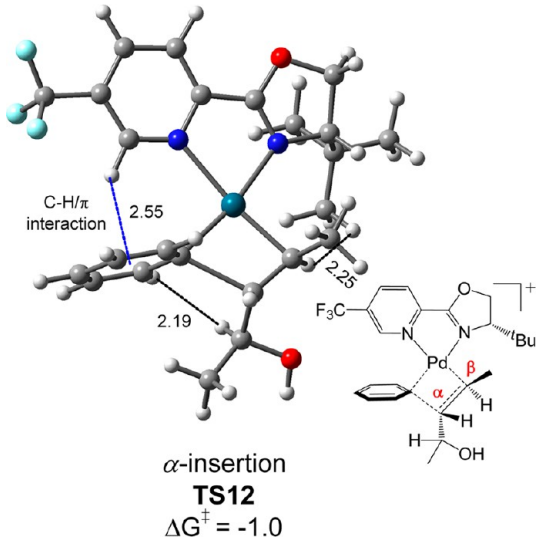

Figure 5. Optimized structure of **TS12** with selected bond distances given in angstroms.

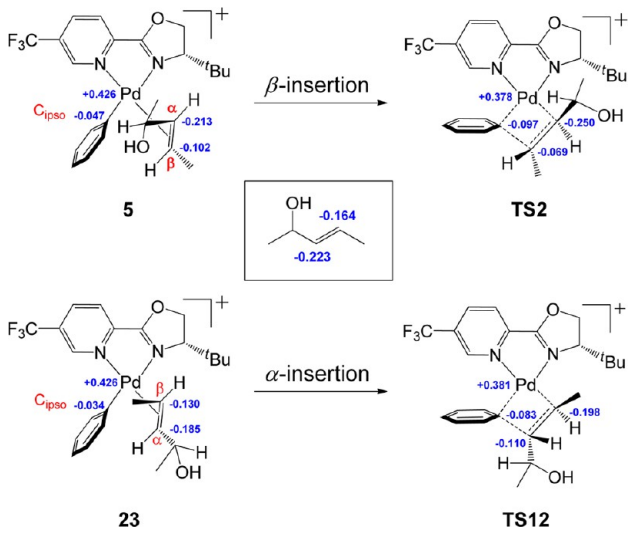

Figure 6. NBO charges on **TS2** and **TS12** and their immediate precursors **5** and **23**.

because it brings about significant C−H/π attractive dispersion forces in **TS2**; that is, one of the C−H bonds on the pyridine points to the center of the phenyl ring at a distance of 2.56 Å. In fact, this kind of C−H/π interaction has been identified previously by numerous computational studies as a differentiating factor (ca. 1.5−2.5 kcal/mol) for the energy of optimized structures.[34] Furthermore, in **TS2** the bulky substituents of $CH(OH)CH_3$ on the metallacycle and *t*-butyl on PyrOx point in opposite directions, thereby reducing steric repulsion. In contrast, **TS4** lacks the C−H/π attractive dispersion forces and suffers steric crowding between the phenyl group and the *t*-butyl substituent on PyrOx, as revealed by the significant C (phenyl)···H (*t*-butyl) repulsion marked at 2.79 Å, which is less than the sum of the van der Waals radii (H 1.20 Å, C 1.70 Å). Stronger H···H steric repulsions also occur in **TS4** than in **TS2**, as indicated by comparing the two sets of shortest nonbonding H···H distances. In addition, NBO charges of PyrOx suggest that the N atom of oxazoline is a somewhat stronger σ donor than the N atom of pyridine.[35] Thus, the Pd−N (oxazoline) bond in **5** has a stronger trans influence than the Pd−N (pyridine) bond in **9** on the anti Pd−C (phenyl) bond that needs breaking in the alkene migratory insertion (Scheme 5), and this contributes in part to the difference in energy between the ensuing transition states **TS2** and **TS4**.

We have discussed the site-selective β-hydride elimination that leads to the β-phenyl ketone **1a** in preference to the typical Heck product **1c**, which is primarily thermodynamic in nature because the carbonyl moiety in **1a** makes it more stable than the isomeric allylic alcohol **1c**. We herein explain the regioselectivity of arylation that favors β-substitution over α-substitution. Of the computed pathways via α-insertion (Supporting Information, Scheme S1), path 5A is the most favorable with the selectivity-controlling alkene migratory insertion transition state **TS12** (Figure 5). On the free energy surface, **TS12** is 3.0 kcal/mol higher than **TS2** of path 1A of β-insertion. The difference explains qualitatively why the α-substituted products were not observed experimentally. Structurally, **TS12** has an important H···H repulsion at 2.19 Å, stronger than any such nonbonding interactions found in **TS2**. Nonetheless, this steric effect alone seems insufficient to explain the difference of 3.0 kcal/mol in energy between **TS2** and **TS12**. Thus, we calculated NBO charges of the key

dx.doi.org/10.1021/ja410118m | J. Am. Chem. Soc. 2014, 136, 986−998

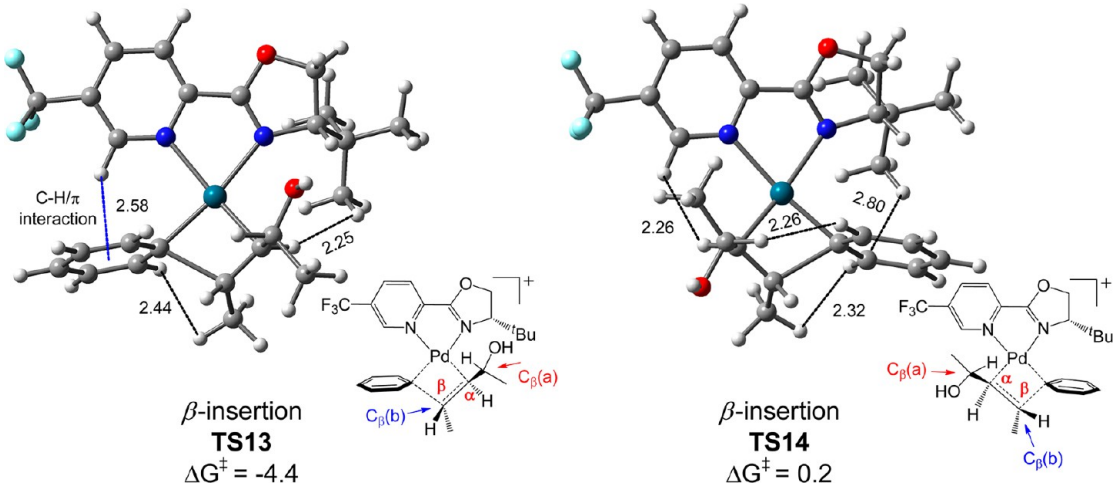

Figure 7. Optimized structures of **TS13** (leading to **1a**) and **TS14** (leading to **1b**) with selected bond distances given in angstroms.

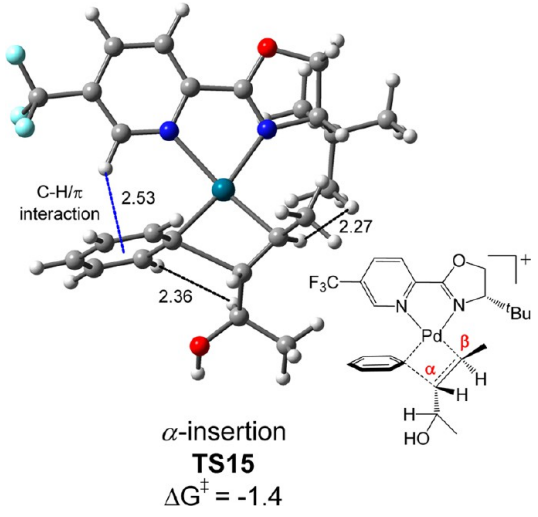

Figure 8. Optimized structure of **TS15** with selected bond distances given in angstroms.

Scheme 6. Reactions Involving (*Z*)- and (*E*)-Allylic Alcohols

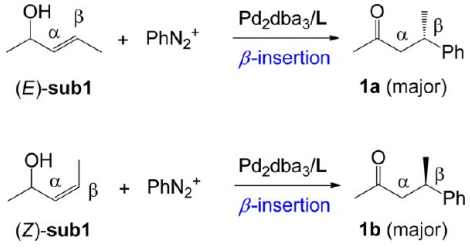

structures to examine bond polarities and their influence on the migratory insertion reactions (Figure 6).

The NBO charges suggest that the Pd−C_α Coulombic attractions in **5** and **TS2** of the β-insertion pathway would be stronger than the analogous Pd−C_β interactions in **23** and **TS12** of the α-insertion pathway. The electron-withdrawing hydroxyl group in the allylic alcohol polarizes the C=C bond, making C_α more negatively charged than C_β, and this is corroborated by the NBO charge analysis of the allylic alcohol in isolated, unbound condition (Figure 6, box). In addition, the Coulombic repulsions between C_{ipso} and C_β in **5** and **TS2** are less than those between C_{ipso} and C_α in **23** and **TS12**. These results from NBO charge analyses are convincing because they agree with the Hammett and ^{13}C chemical shift studies by Sigman et al.[20] Thus, the electronic effects, coupled with the above-mentioned steric factor, give a qualitative explanation for the difference in energy between **TS2** and **TS12** and the regioselectivity thereof that favors β-insertion over α-insertion.

For comparison purposes, we also calculated the key transition states of **TS2**, **TS4**, and **TS12** with M06/BS2//M06/BS1, and their optimized geometries and relative energies are in good agreement with those obtained from calculations with M06/BS2//B3LYP/BS1 (Supporting Information, Figure S3).

Because experimentally a racemate of (*E*)-(*R*)-**sub1** and (*E*)-(*S*)-**sub1** was used and found not to bias the reaction selectivities, we further investigated various reaction pathways (paths 1B−8B) using (*E*)-(*R*)-**sub1** (Supporting Information, Schemes S2 and S3). The controlling alkene migratory insertion transition states for the most favorable pathways to **1a** and **1b** are, respectively, **TS13** and **TS14**, whose optimized structures are shown in Figure 7. **TS13** and **TS14** are correspondingly analogous to **TS2** and **TS4** stemming from (*E*)-(*S*)-**sub1**, and all four of them are diastereomeric with one another. The structural difference between **TS13** and **TS2** or between **TS14** and **TS4** is small, only in the transposition of the OH and CH_3 groups on the C_β(a) atom. This explains the small difference in energy between **TS13** and **TS2** or between **TS14** and **TS4**. Just as **TS2** is lower than **TS4** (Figure 4), so similar structural differences make **TS13** more stable than **TS14** by 4.6 kcal/mol, from which the enantioselectivity arises favoring **1a** over **1b**. In addition, **TS15** (Figure 8) is the controlling alkene insertion barrier for the most favorable pathway of α-insertion involving (*E*)-(*R*)-**sub1**, which is analogous to **TS12** stemming from (*E*)-(*S*)-**sub1**. **TS15** is 3.0 kcal/mol higher than **TS13** of the β-insertion involving (*E*)-(*R*)-**sub1**, and the difference suggests that the α-substituted products essentially would not be generated from (*E*)-(*R*)-**sub1**. In summary, our computational results explain why a racemate of allylic alcohol can be used without biasing the enantio- and regioselectivities of arylation.

Reactions Involving (Z)-Alkene Substrates. Experimentally, a (*Z*)-allylic alcohol substrate gives the opposite enantiomer of product, as shown in Schemes 2 (eq 1 vs eq 2) and 6. To explain this interesting result, we explored the reactions with (*Z*)-**sub1** and compared them to those involving (*E*)-**sub1**

dx.doi.org/10.1021/ja410118m | J. Am. Chem. Soc. 2014, 136, 986−998

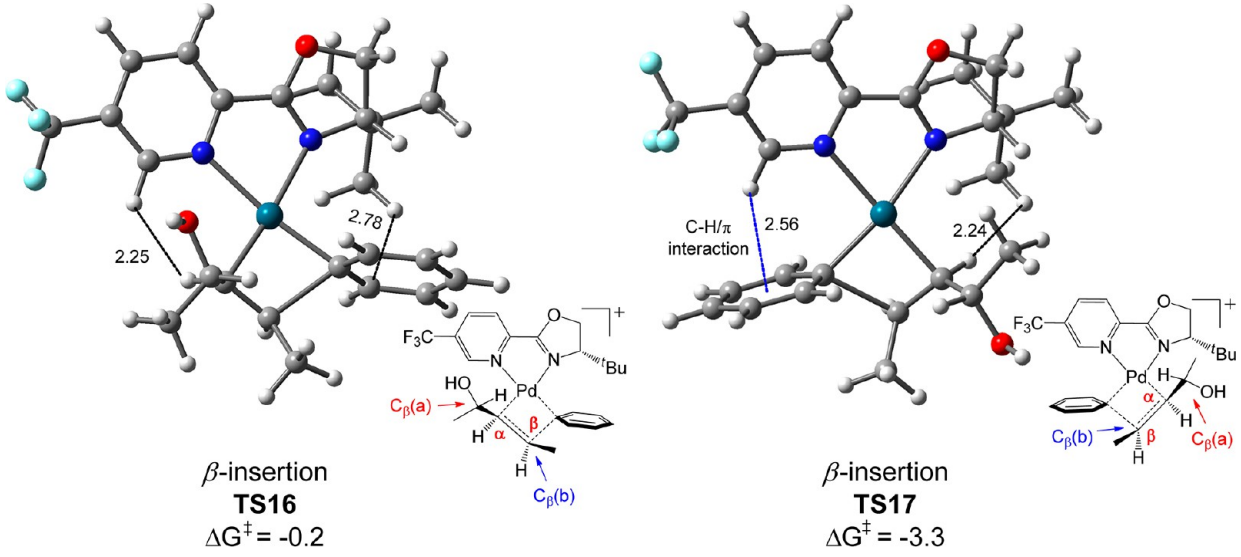

Figure 9. Optimized structures of **TS16** (leading to **1a**) and **TS17** (leading to **1b**) with selected bond distances given in angstroms.

Scheme 7. The Heck Arylation of Alkenyl Alcohol

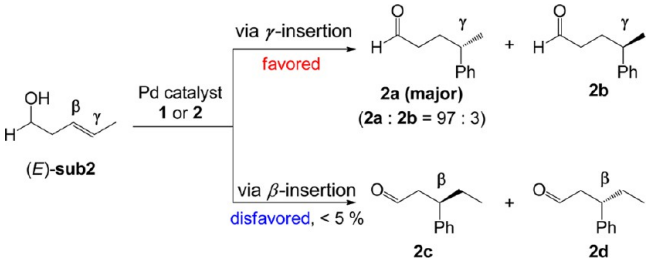

(Supporting Information, Schemes S4−8 and Figure S4). For each pathway involving (*Z*)-**sub1** (Supporting Information, paths 1C−8C and 1D−8D), the alkene migratory insertion is a key step that controls both the regio- and the enantioselectivities. The controlling alkene insertion transition states for the most favorable pathways of (*Z*)-(*S*)-**sub1** to **1a** and **1b** are, respectively, **TS16** and **TS17** (Figure 9). **TS16** and **TS17** correspond to **TS4** and **TS2** (Figure 4) stemming from (*E*)-(*S*)-**sub1**, all of them being diastereomers with one another. Just as **TS2** is more stable than **TS4** because of the significant structural differences, so too is **TS17** more stable than **TS16**. The difference in energy (3.1 kcal) between **TS16** and **TS17** gives rise to an enantioselectivity favoring **1b** over **1a**. The

Scheme 8. The Most Favorable Pathways for (*E*)-sub2 with Pd Catalyst 1 or 2 Leading to 2a−2d

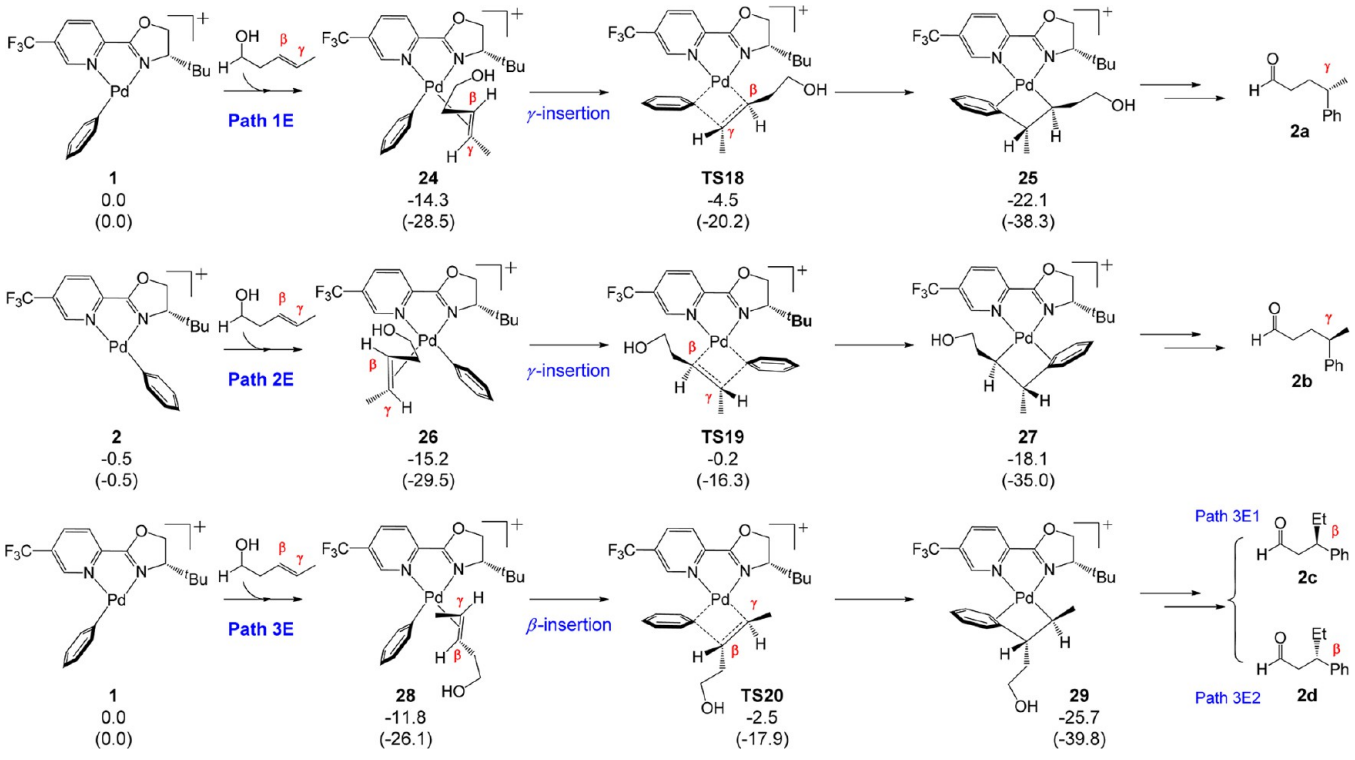

dx.doi.org/10.1021/ja410118m | J. Am. Chem. Soc. 2014, 136, 986−998

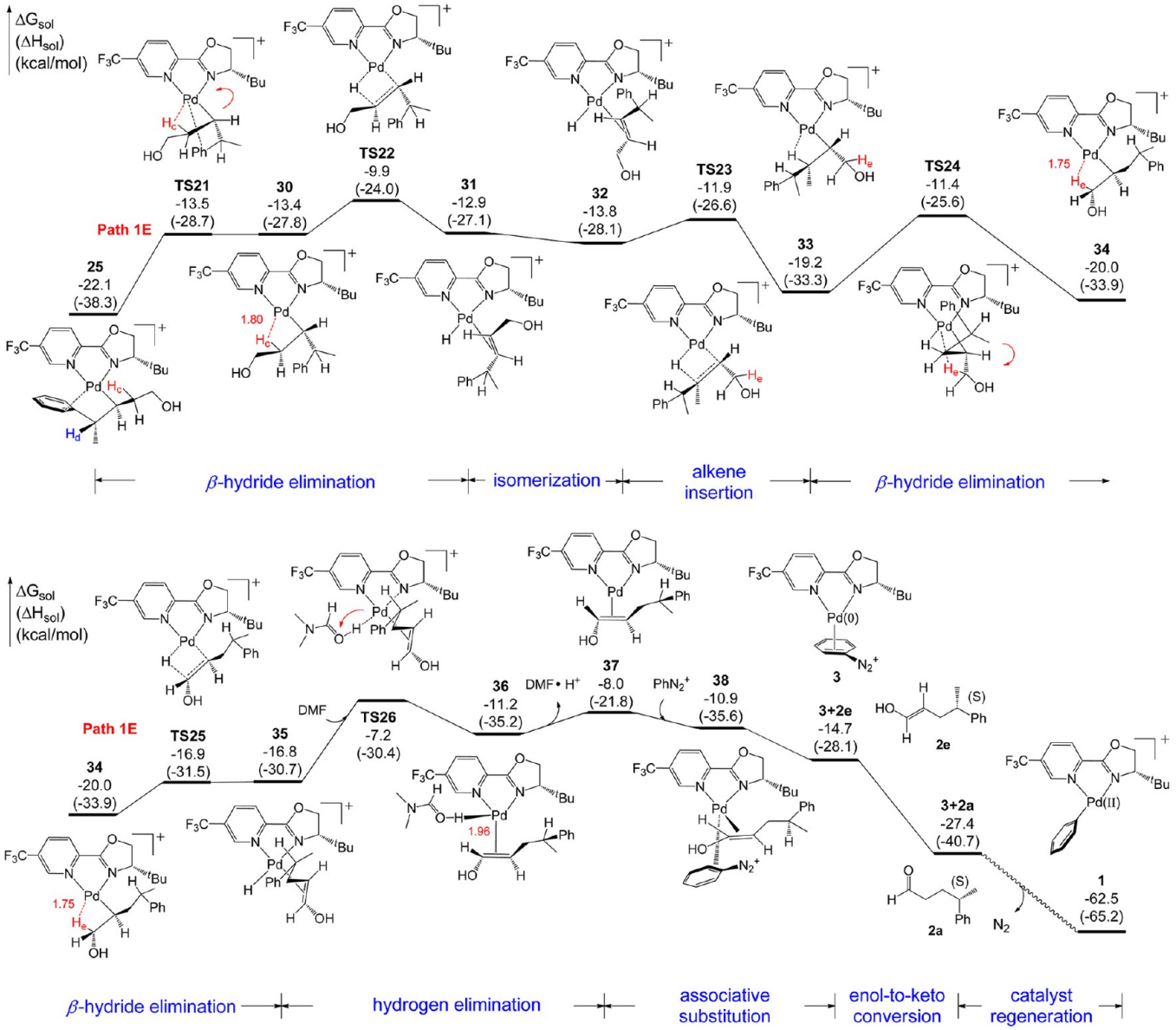

Figure 10. Free energy profile for the reaction of Pd catalyst **1** with (*E*)-**sub2** leading to the (*S*)-γ-phenyl keto product **2a**. Note that the pathway involving β-H_d elimination from **25** leading to the typical Heck product has also been considered (see Figure S6 in the Supporting Information for details).

structural difference between **TS17** and **TS2** is in the transposition of the H and CH_3 groups on the C_β(b) atom, and this explains the opposing enantioselectivities observed for the reactions involving (*E*)-(*S*)-**sub1** and (*Z*)-(*S*)-**sub1**, which give **1a** and **1b** as the major products, respectively. Calculations on the reaction with (*Z*)-(*R*)-**sub1** also gave **1b** as the major product (Supporting Information, Schemes S7 and S8).

3.3. Reactions with Alkenyl Alcohols. This Heck-type reaction not only produces enantioselective β-aryl ketones as discussed above, but it also allows direct access to enantioselective γ- or δ-substituted aryl carbonyl products from alkenyl alcohol substrates (eqs 3–5, Scheme 2), a transformation that is hardly achievable by other asymmetric catalytic methods.[18] To elucidate this remarkable reactivity that combines stereoselectivity and the C=C bond relay, we performed DFT calculations on a reaction of eq 3 using (*E*)-**sub2** as substrate, whose experimentally observed products and selectivities are shown in Scheme 7.

Mechanism. By analogy with the (*E*)-(*S*)-**sub1** system (Schemes 5 and Supporting Information S1), we explored eight possible alkene insertion pathways for the reactions of (*E*)-**sub2** with Pd catalyst **1** or **2** (Supporting Information, Schemes S9 and S10). For each pathway, the transition state of alkene migratory insertion controls both the regio- and the enantioselectivities, and the most favorable pathways leading to **2a**–**2d** are summarized in Scheme 8. Path 1E leads to the major product **2a**, the details of which are discussed here. As shown in Scheme 8, path 1E begins with coordination of (*E*)-**sub2**, forming the π complex **24** with the γ-carbon atom oriented toward the phenyl group on the palladium center to facilitate the subsequent γ-insertion via **TS18** that progresses to the 16-electron palladium alkyl complex **25** with a Pd–η^2-phenyl bond.

The free energy profile of path 1E from **25** onward is shown in Figure 10. Complex **25** isomerizes through Pd–C_α bond rotation via **TS21**, affording complex **30** with an agostic Pd–H_c

dx.doi.org/10.1021/ja410118m | J. Am. Chem. Soc. 2014, 136, 986–998

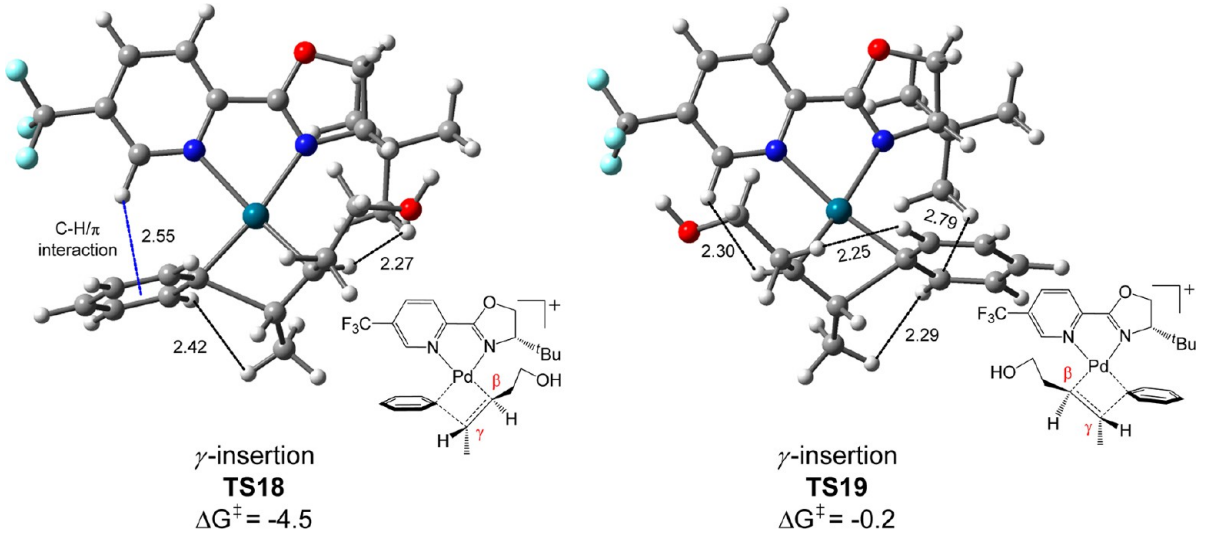

Figure 11. Optimized structures of **TS18** (leading to **2a**) and **TS19** (leading to **2b**) with selected distances given in angstroms.

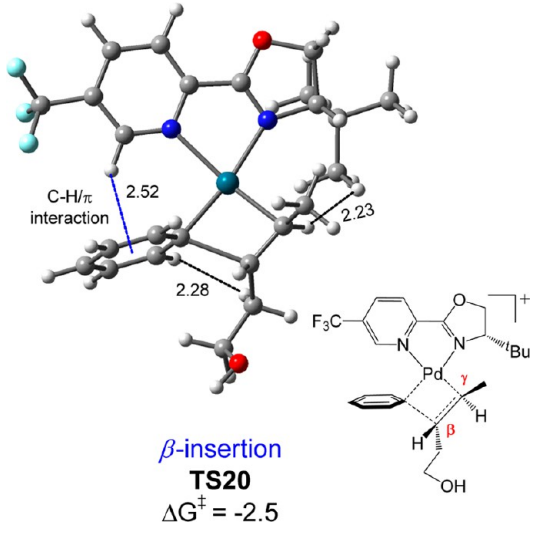

Figure 12. Optimized structure of **TS20** with selected distances given in angstroms.

interaction at 1.80 Å, which then undergoes β–H_c elimination via **TS22** to form the intermediate **31** with the (*S*)-allylic alcohol product π-bound to the palladium center. Complex **31**, however, could not introduce the C═C bond relay, as its alkene migratory insertion would revert to **30**. Thus, we located the isomeric complex **32**, which would result from dissociation of the alkene ligand from **31**, followed by rebinding of the alkene to the palladium center with a different orientation. Note that the **31** to **32** conversion is thermodynamically favorable (ΔG^0 = −0.9 kcal/mol). The alkene ligand in complex **32** undergoes migratory insertion into the Pd–H bond via **TS23** to give complex **33**, and this step is both kinetically facile with a low activation energy (1.9 kcal/mol) and thermodynamically favorable with ΔG^0 = −5.4 kcal/mol. Complex **33** isomerizes via Pd–C_α bond rotation (**TS24**), forming **34** that has a Pd–C–C–H_f dihedral angle at 14.3° and an agostic Pd–H_f interaction at 1.75 Å to enable the following β-hydride elimination. The β-hydride elimination proceeds via **TS25** to give complex **35** with the π-bound (*S*)-enol product **2e**, thereby realizing the C═C bond relay toward the alcohol end. The release of the π-bound **2e** from complex **35** follows the same mechanism as computed for complexes **14** and **19** (Figure 3), beginning with a DMF-mediated deprotonation via **TS26** to generate a formal Pd(0) complex (**36**) that discharges DMF·H^+ to form complex **37**. Complex **37** then undergoes associative substitution for phenyldiazonium through the four-coordinate, tetrahedral intermediate **38** to lead to the original Pd(0) complex **3** and the (*S*)-enol product **2e**. The (*S*)-enol **2e** tautomerizes to the (*S*)-γ-phenyl keto product **2a** by a large thermodynamic driving force of 12.7 kcal/mol (Supporting Information, Figure S5). Complex **3** undergoes oxidation by the phenyldiazonium cation PhN_2^+ to regenerate the active catalyst **1**, as discussed above (Figures 2 and 3). The γ-phenyl keto product **2a** is thermodynamically more stable by 16.2 kcal/mol than the allylic alcohol in **31** that would be the alternative product, and this is the driving force for the C═C bond migration toward the alcohol end and hence the formation of the final product **2a**.

Origins of Regio- and Enantioselectivities. The selectivity-controlling TSs for the most favorable γ-insertion pathways

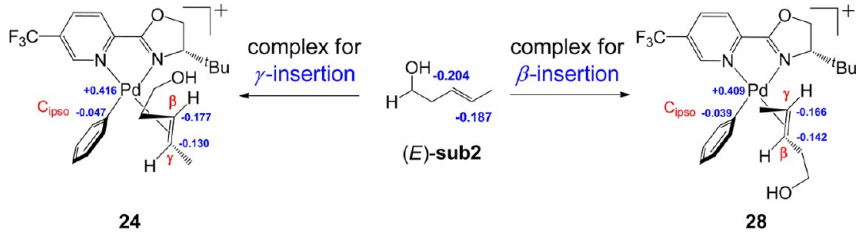

Figure 13. NBO charges on the precursors of **TS18** (γ-insertion) and **TS20** (β-insertion).

dx.doi.org/10.1021/ja410118m | J. Am. Chem. Soc. 2014, 136, 986–998

Scheme 9. Catalytic Cycle for the Heck Arylation of Allylic and Alkenyl Alcohols

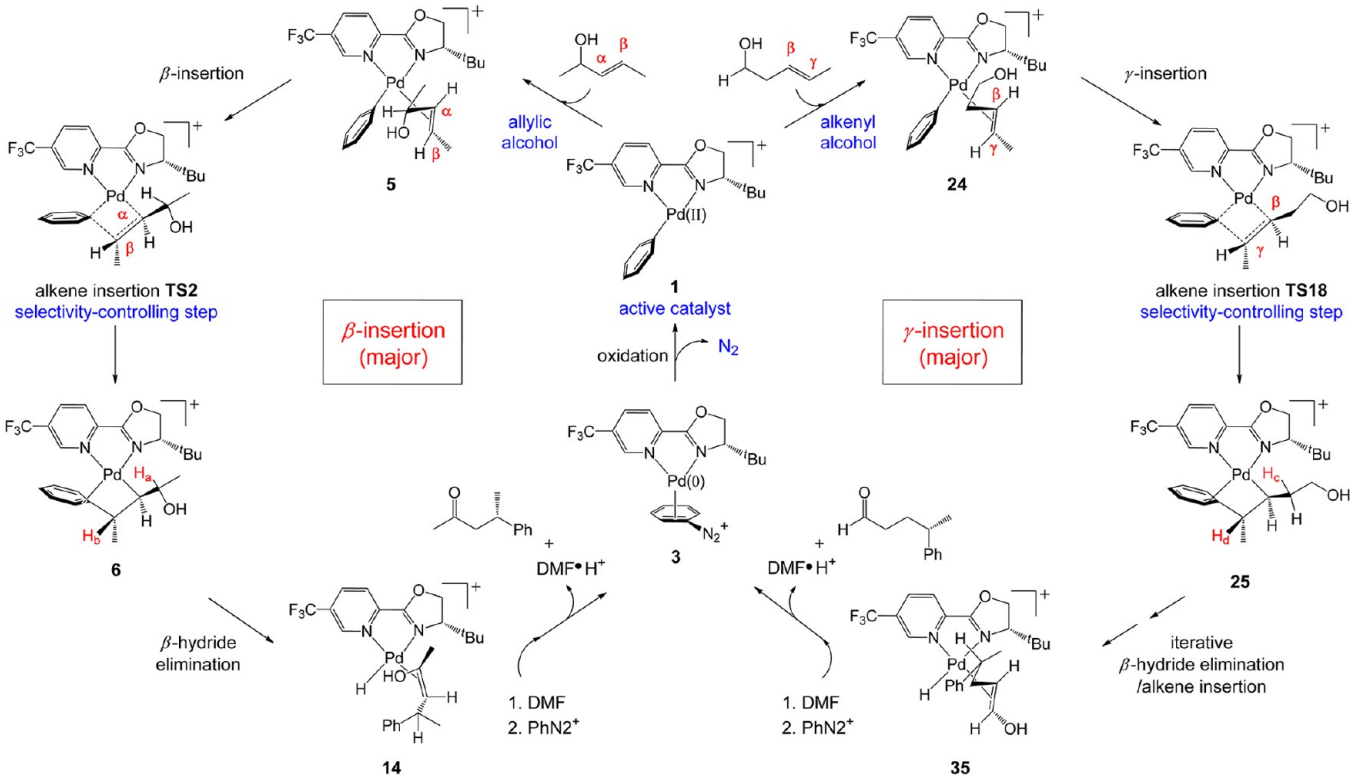

leading to **2a** (path 1E) and **2b** (path 2E) are respectively **TS18** and **TS19**, with optimized structures shown in Figure 11. **TS18** and **TS19** are, respectively, analogous to **TS2** and **TS4** stemming from (*E*)-(*S*)-**sub1** (Figure 4). On account of a combination of steric repulsion, trans influence, and C−H/π dispersion forces, **TS18** is lower by 4.3 kcal/mol than **TS19**, which agrees with the experimentally observed enantioselectivity (**2a**:**2b** = 97:3). The selectivity-controlling alkene insertion transition state for the most favored β-insertion course is **TS20** (Figure 12), which would lead to **2c** and **2d** (Supporting Information, Schemes S10,S11 and Figure S7).

That this Heck-type reaction favors γ-insertion over β-insertion is attributed to the gap (2.0 kcal/mol) between **TS18** and **TS20**, which gives a calculated γ-selectivity of 96.7% that is consistent with the experimental results (<5% products of β-insertion). We have explained above why the β-insertion is favored over the α-insertion (Figures 4−6), and this regioselectivity results from a combination of electronic and steric effects. Similar structural factors appear to set apart **TS20** and **TS18** energetically. As compared to **TS18**, **TS20** has an extra significant steric H···H repulsion at 2.28 Å (Figures 11 and 12). In addition, NBO charges on the precursors (**24** and **28**) to **TS18** and **TS20** suggest that the Pd−C_β Coulombic attraction in **24** of the γ-insertion pathway is stronger than the analogous Pd−C_γ attraction in **28** of the β-insertion pathway (Figure 13). The electron-withdrawing hydroxyl group in (*E*)-**sub2** makes C_β more negatively charged than C_γ (Figure 13). Because the hydroxyl group is one more carbon atom away from the C=C bond in (*E*)-**sub2** than in (*E*)-**sub1**, the electronic effect in (*E*)-**sub2** is weaker, giving a smaller ΔTS_{20-18} (2.0 kcal/mol) as compared to ΔTS_{12-2} (3.0 kcal/mol). This is reflected on the fact that the γ-selectivity (95%, γ vs β) is less than the β-selectivity (100%, β vs α). It follows that this electronic effect would be further weakened in the alkenyl alcohol system with a longer carbon chain (eq 5, Scheme 2), for which the energy difference in the key TSs of the alkene migratory insertion is 1.1 kcal/mol, giving a calculated regioselectivity (δ:γ = 6.4:1) that is consistent with experimental values (δ:γ = 4:1) (Supporting Information, Schemes S12 and Figure S8). Thus, our computational results successfully explain the favored direction of the alkene migratory insertion; that is, the aryl group selectively attacks the sp^2-C atom that is distal from the alcohol end (Scheme 2). In addition, our results explain the observed trend that the distal regioselectivity decreases with increasing carbon chain length of the alkenyl alcohol (Scheme 2, eq 1 vs eq 3 vs eq 5).

4. CONCLUSION

We have presented a detailed DFT study on the mechanism and origins of regio- and enantioselectivities of the palladium/PyrOx-catalyzed Heck-type relay arylations of allylic and alkenyl alcohols. For every reaction that we have explored, the major product is derived from active catalyst **1** rather than **2**. This is because catalyst **1** leads to four-coordinate transition states with relatively favorable configurations to allow C−H/π attractive dispersion forces and avoid steric repulsion of the phenyl group with the *t*-butyl group on the ligand (see below). Scheme 9 summarizes the reaction sequence and depicts the catalytic cycle.

For the Heck arylation of allylic alcohols, the catalytic cycle involves oxidation of Pd(0) to Pd(II) by the aryldiazonium source, alkene migratory insertion, β-hydride elimination, and DMF-mediated reductive hydride elimination. The alkene migration insertion is the crucial step, which controls both the regio- and the enantioselectivities of arylation. The enantioselectivity stems from a combination of steric repulsion, trans influence, and C−H/π dispersion forces. In the key transition states of alkene insertion (e.g., **TS2**), the cis phenyl

dx.doi.org/10.1021/ja410118m | J. Am. Chem. Soc. 2014, 136, 986−998

orientation toward the pyridine moiety of PyrOx enables C−H/π dispersion interactions, and the bulky substituents of $CH(OH)CH_3$ and *t*-butyl point away from each other to reduce steric congestion. The distal β-regioselectivity arises from a combination of steric repulsions and the electronic effect of the hydroxyl group on the charge distribution over the C_α=C_β bond (e.g., **TS2** vs **TS12**). A racemate of an allylic alcohol can be used without biasing the regio- and enantioselectivities because the (*R*) and (*S*) enantiomorphs give intermediates and TSs with closely similar energies. The origins of the opposite enantiomers of product generated from (*E*)- and (*Z*)-alkene substrates lie in the transposition of the H and CH_3 groups on the prochiral C_β(b) atom of the key alkene insertion transition states (e.g., **TS2** vs **TS17**).

For the Heck arylation of alkenyl alcohols, the catalytic cycle includes an iterative alkene migratory insertion/β-hydride elimination process, in which the C=C bond moves toward the alcohol end, ultimately resulting in the thermodynamically more stable carbonyl product via enol-to-keto conversion. The origins of the regio- and enantioselectivites of arylation are analogous to those found for the reactions involving allylic alcohols. The distal regioselectivity decreases with increasing carbon chain length and diminishing electronic effect of the hydroxyl group.

The results taken together help us understand this new Heck-type reaction. The Pd−PyrOx chelate framework of the catalyst differentiates by ways of steric repulsion and C−H/π attractive dispersion forces the energies of key TSs with substituents in different orientations toward the framework. In addition, the electronic effect of the hydroxyl group in the allylic/alkenyl alcohol substrates contributes to the distal regioselectivity by polarizing the C=C double bond. These insights will be useful to the further development of Heck-type reactions.

■ ASSOCIATED CONTENT

Supporting Information

Additional computational results and the complete ref 31. This material is available free of charge via the Internet at http://pubs.acs.org.

■ AUTHOR INFORMATION

Corresponding Authors

zxwang@ucas.ac.cn

xiaotai.wang@ucdenver.edu

Notes

The authors declare no competing financial interest.

■ ACKNOWLEDGMENTS

We acknowledge support for this work from the Chinese Academy of Science, the National Science Foundation of China (Grant nos. 20973197 and 21173263), and the University of Colorado, Denver.

■ REFERENCES

(1) (a) Heck, R. F. *J. Am. Chem. Soc.* **1969**, *91*, 6707. (b) Heck, R. F.; Nolley, J. P., Jr. *J. Org. Chem.* **1972**, *37*, 2320. (c) Heck, R. F. In *Comprehensive Organic Synthesis*; Trost, B. M., Fleming, I., Eds.; Pergamon Press: Oxford, 1991; Vol. 4. (d) Demeijere, A.; Meyer, F. E. *Angew. Chem., Int. Ed. Engl.* **1995**, *33*, 2379. (e) Shibasaki, M.; Vogl, E. M. *J. Organomet. Chem.* **1999**, *576*, 1. (f) Beletskaya, I. P.; Cheprakov, A. V. *Chem. Rev.* **2000**, *100*, 3009.

(2) Hartwig, J. F. *Organotransition Metal Chemistry: From Bonding to Catalysis*; University Science Books: Herndon, VA, 2010.

(3) (a) Cabri, W.; Candiani, I. *Acc. Chem. Res.* **1995**, *28*, 2. (b) Ruan, J.; Xiao, J. *Acc. Chem. Res.* **2011**, *44*, 614.

(4) (a) Dounay, A. B.; Overman, L. E. *Chem. Rev.* **2003**, *103*, 2945. (b) Shibasaki, M.; Vogl, E. M.; Ohshima, T. *Adv. Synth. Catal.* **2004**, *346*, 1533. (c) McCartney, D.; Guiry, P. *J. Chem. Soc. Rev.* **2011**, *40*, 5122.

(5) (a) Xue, L.; Lin, Z. *Chem. Soc. Rev.* **2010**, *39*, 1692. (b) Knowles, J. P.; Whiting, A. *Org. Biomol. Chem.* **2007**, *5*, 31.

(6) Albert, K.; Gisdakis, P.; Rösch, N. *Organometallics* **1998**, *17*, 1608.

(7) Lee, M.-T.; Lee, H. M.; Hu, C.-H. *Organometallics* **2007**, *26*, 1317.

(8) (a) Surawatanawong, P.; Fan, Y.; Hall, M. B. *J. Organomet. Chem.* **2008**, *693*, 1552. (b) Surawatanawong, P.; Hall, M. B. *Organometallics* **2008**, *27*, 6222.

(9) Deeth, R. J.; Smith, A.; Brown, J. M. *J. Am. Chem. Soc.* **2004**, *126*, 7144.

(10) Henriksen, S. T.; Norrby, P.-O.; Kaukoranta, P. i.; Andersson, P. G. *J. Am. Chem. Soc.* **2008**, *130*, 10414.

(11) (a) Fristrup, P.; Le Quement, S.; Tanner, D.; Norrby, P.-O. *Organometallics* **2004**, *23*, 6160. (b) Ahlquist, M.; Fristrup, P.; Tanner, D.; Norrby, P.-O. *Organometallics* **2006**, *25*, 2066. (c) Ahlquist, M.; Norrby, P.-O. *Organometallics* **2007**, *26*, 550. (d) Ambrogio, I.; Fabrizi, G.; Cacchi, S.; Henriksen, S. T.; Fristrup, P.; Tanner, D.; Norrby, P.-O. *Organometallics* **2008**, *27*, 3187. (e) Henriksen, S. T.; Tanner, D.; Cacchi, S.; Norrby, P.-O. *Organometallics* **2009**, *28*, 6201.

(12) Gøgsig, T. M.; Kleimark, J.; Nilsson Lill, S. O.; Korsager, S.; Lindhardt, A. T.; Norrby, P.-O.; Skrydstrup, T. *J. Am. Chem. Soc.* **2012**, *134*, 443.

(13) (a) Legault, C. Y.; Garcia, Y.; Merlic, C. A.; Houk, K. N. *J. Am. Chem. Soc.* **2007**, *129*, 12664. (b) Lan, Y.; Houk, K. N. *J. Org. Chem.* **2011**, *76*, 4905. (c) Lan, Y.; Liu, P.; Newman, S. G.; Lautens, M.; Houk, K. N. *Chem. Sci.* **2012**, *3*, 1987.

(14) (a) Lan, Y.; Deng, L.; Liu, J.; Wang, C.; Wiest, O.; Yang, Z.; Wu, Y.-D. *J. Org. Chem.* **2009**, *74*, 5049. (b) Peng, Q.; Yan, H.; Zhang, X.; Wu, Y.-D. *J. Org. Chem.* **2012**, *77*, 7487.

(15) Werner, E. W.; Mei, T.-S.; Burckle, A. J.; Sigman, M. S. *Science* **2012**, *338*, 1455.

(16) Examples of using pyridine/quinoline oxazoline ligands in Pd-catalyzed reactions: (a) Zhang, Y.; Sigman, M. S. *J. Am. Chem. Soc.* **2007**, *129*, 3076. (b) Michel, B. W.; Camelio, A. M.; Cornell, C. N.; Sigman, M. S. *J. Am. Chem. Soc.* **2009**, *131*, 6076. (c) Jensen, K. H.; Pathak, T. P.; Zhang, Y.; Sigman, M. S. *J. Am. Chem. Soc.* **2009**, *131*, 17074. (d) McDonald, R. I.; White, P. B.; Weinstein, A. B.; Tam, C. P.; Stahl, S. S. *Org. Lett.* **2011**, *13*, 2830. (e) Kikushima, K.; Holder, J. C.; Gatti, M.; Stoltz, B. M. *J. Am. Chem. Soc.* **2011**, *133*, 6902. (f) Michel, B. W.; Steffens, L. D.; Sigman, M. S. *J. Am. Chem. Soc.* **2011**, *133*, 8317. (g) Sigman, M. S.; Werner, E. W. *Acc. Chem. Res.* **2012**, *45*, 874. (h) Holder, J. C.; Zou, L.; Marziale, A. N.; Liu, P.; Lan, Y.; Gatti, M.; Kikushima, K.; Houk, K. N.; Stoltz, B. M. *J. Am. Chem. Soc.* **2013**, *135*, 14996.

(17) Allylic and alkenyl alcohols are defined as having the skeletons HO−C−C=C− and HO−$(C)_n$−C=C− ($n \geq 2$), respectively.

(18) (a) Smith, S. W.; Fu, G. C. *J. Am. Chem. Soc.* **2009**, *131*, 14231. (b) Zultanski, S. L.; Fu, G. C. *J. Am. Chem. Soc.* **2011**, *133*, 15362.

(19) Gilbertson, S. R. *Science* **2012**, *338*, 1432.

(20) Mei, T.-S.; Werner, E. W.; Burckle, A. J.; Sigman, M. S. *J. Am. Chem. Soc.* **2013**, *135*, 6830.

(21) Examples of isomerization/migration in Heck-type reactions: (a) Wang, Y.; Dong, X.; Larock, R. C. *J. Org. Chem.* **2003**, *68*, 3090. (b) Berthiol, F.; Doucet, H.; Santelli, M. *Tetrahedron* **2006**, *62*, 4372. (c) Crawley, M. L.; Phipps, K. M.; Goljer, I.; Mehlmann, J. F.; Lundquist, J. T.; Ullrich, J. W.; Yang, C.; Mahaney, P. E. *Org. Lett.* **2009**, *11*, 1183. (d) Kochi, T.; Hamasaki, T.; Aoyama, Y.; Kawasaki, J.; Kakiuchi, F. *J. Am. Chem. Soc.* **2012**, *134*, 16544.

(22) (a) Lee, C. T.; Yang, W. T.; Parr, R. G. *Phys. Rev. B* **1988**, *37*, 785. (b) Becke, A. D. *J. Chem. Phys.* **1993**, *98*, 5648.

(23) Marenich, A. V.; Cramer, C. J.; Truhlar, D. G. *J. Phys. Chem. B* **2009**, *113*, 6378.
(24) (a) Andrae, D.; Häussermann, U.; Dolg, M.; Stoll, H.; Preuss, H. *Theor. Chim. Acta* **1990**, *77*, 123. (b) Roy, L. E.; Hay, P. J.; Martin, R. L. *J. Chem. Theory Comput.* **2008**, *4*, 1029.
(25) Zhao, Y.; Truhlar, D. G. *Theor. Chem. Acc.* **2008**, *120*, 215.
(26) (a) Zhao, Y.; Truhlar, D. G. *Acc. Chem. Res.* **2008**, *41*, 157. (b) Kulkarni, A. D.; Truhlar, D. G. *J. Chem. Theory Comput.* **2011**, *7*, 2325. (c) Zhao, Y.; Truhlar, D. G. *J. Chem. Theory Comput.* **2009**, *5*, 324.
(27) (a) Benitez, D.; Shapiro, N. D.; Tkatchouk, E.; Wang, Y. M.; Goddard, W. A., III; Toste, F. D. *Nat. Chem.* **2009**, *1*, 482. (b) Benitez, D.; Tkatchouk, E.; Goddard, W. A., III. *Organometallics* **2009**, *28*, 2643. (c) Sieffert, N.; Bühl, M. *Inorg. Chem.* **2009**, *48*, 4622. (d) Ariafard, A.; Hyland, C. J. T.; Canty, A. J.; Sharma, M.; Yates, B. F. *Inorg. Chem.* **2011**, *50*, 6449. (e) Dang, Y.; Qu, S.; Wang, Z.-X.; Wang, X. *Organometallics* **2013**, *32*, 2804.
(28) (a) Liu, P.; Xu, X.; Dong, X.; Keitz, B. K.; Herbert, M. B.; Grubbs, R. H.; Houk, K. N. *J. Am. Chem. Soc.* **2012**, *134*, 1464. (b) Herbert, M. B.; Lan, Y.; Keitz, B. K.; Liu, P.; Endo, K.; Day, M. W.; Houk, K. N.; Grubbs, R. H. *J. Am. Chem. Soc.* **2012**, *134*, 7861. (c) Giri, R.; Lan, Y.; Liu, P.; Houk, K. N.; Yu, J.-Q. *J. Am. Chem. Soc.* **2012**, *134*, 14118. (d) Miyazaki, H.; Herbert, M. B.; Liu, P.; Dong, X.; Xu, X.; Keitz, B. K.; Ung, T.; Mkrtumyan, G.; Houk, K. N.; Grubbs, R. H. *J. Am. Chem. Soc.* **2013**, *135*, 5848. (e) Hong, X.; Trost, B. M.; Houk, K. N. *J. Am. Chem. Soc.* **2013**, *135*, 6588. (f) Xu, X.; Liu, P.; Shu, X.-z.; Tang, W.; Houk, K. N. *J. Am. Chem. Soc.* **2013**, *135*, 9271.
(29) (a) Tang, S.-Y.; Guo, Q.-X.; Fu, Y. *Chem.—Eur. J.* **2011**, *17*, 13866. (b) Ariafard, A.; Asadollah, E.; Ostadebrahim, M.; Rajabi, N. A.; Yates, B. F. *J. Am. Chem. Soc.* **2012**, *134*, 16882.
(30) (a) Dang, Y.; Wang, Z.-X.; Wang, X. *Organometallics* **2012**, *31*, 7222. (b) Dang, Y.; Wang, Z.-X.; Wang, X. *Organometallics* **2012**, *31*, 8654. (c) Qu, S.; Dang, Y.; Wen, M.; Wang, Z.-X. *Chem.—Eur. J.* **2013**, *19*, 3827.
(31) Frisch, M. J.; et al. *Gaussian 09*, revision A.01; Gaussian, Inc.: Wallingford, CT, 2009.
(32) Jiao, L.; Lin, M.; Yu, Z.-X. *J. Am. Chem. Soc.* **2011**, *133*, 447.
(33) The direct dissociations of the enol **1d** from complexes **14** and **16** would be highly endergonic by 19.4 and 24.9 kcal/mol, respectively (see Scheme S13 in the Supporting Information).
(34) (a) Takatani, T.; Sherrill, C. D. *Phys. Chem. Chem. Phys.* **2007**, *9*, 6106. (b) Xu, X.; Liu, P.; Lesser, A.; Sirois, L. E.; Wender, P. A.; Houk, K. N. *J. Am. Chem. Soc.* **2012**, *134*, 11012. (c) Krenske, E. H.; Houk, K. N. *Acc. Chem. Res.* **2013**, *46*, 979.
(35) NBO charges: N (oxazoline) = −0.538 and N (pyridine) = −0.471.